A Journal of the Gesellschaft Deutscher Chemiker

Angewandte International Edition GDCh Chemie

www.angewandte.org

Accepted Article

Title: Self-Assembly of Highly Stable Zirconium (IV) Coordination Cages with Aggregation Induced Emission (AIE) Molecular Rotors for Live-Cell Imaging

Authors: Jinqiao Dong, Yutong Pan, Heng Wang, Kuiwei Yang, Lingmei Liu, Zhiwei Qiao, Yi Di Yuan, Shing Bo Peh, Jian Zhang, Leilei Shi, Hong Liang, Yu Han, Xiaopeng Li, Jianwen Jiang, Bin Liu, and Dan Zhao

To be cited as: *Angew. Chem. Int. Ed.* 10.1002/anie.201915199
Angew. Chem. 10.1002/ange.201915199

Link to VoR: http://dx.doi.org/10.1002/anie.201915199
http://dx.doi.org/10.1002/ange.201915199

WILEY-VCH

10.1002/anie.201915199

WILEY-VCH

RESEARCH ARTICLE

Self-Assembly of Highly Stable Zirconium (IV) Coordination Cages with Aggregation Induced Emission (AIE) Molecular Rotors for Live-Cell Imaging

Jinqiao Dong,[+][a] Yutong Pan,[+][a] Heng Wang,[b] Kuiwei Yang,[a] Lingmei Liu,[c] Zhiwei Qiao,[d] Yi Di Yuan,[a] Shing Bo Peh,[a] Jian Zhang,[a] Leilei Shi,[a] Hong Liang,[d] Yu Han,[c] Xiaopeng Li,[b] Jianwen Jiang,[a] Bin Liu,*[a] and Dan Zhao*[a]

This paper is dedicated to the 20 Anniversary of Aggregation Induced Emission (AIE)

Abstract: Although supramolecular coordination complexes have demonstrated outstanding host-guest chemistry in solution or solid state, the low structural stability, weak fluorescence emission, and cell viability in aqueous solutions have limited their applications in real cellular environment. Herein, we report the self-assembly of highly stable zirconium (IV)-based coordination cages with aggregation induced emission (AIE) molecular rotors for in-vitro bio-imaging. The two coordination cages, viz. NUS-100 and NUS-101, are assembled from the highly stable trinuclear zirconium vertices and two flexible carboxyl-decorated tetraphenylethylene (TPE) spacers. Extensive experimental and theoretical results show that the emissive intensity of the coordination cages can be controlled by restricting the dynamics of AIE-active molecular rotors though multiple external stimuli. Because the two coordination cages have excellent chemical stability in aqueous solutions (pH stability: 2 – 10) and impressive AIE characteristics contributed by the molecular rotors, they can be employed as novel biological fluorescent probes for in-vitro live-cell imaging.

Introduction

Coordination-driven self-assembly has emerged as a powerful bottom-up approach to construct artificial supramolecular coordination complexes (SCCs) with well-defined sizes and shapes,[1] as well as functionality for mimicking host-guest recognition in living organisms.[2] SCCs have garnered great interest in the past two decades as enzyme mimetics, with advanced functions and potential applications in anion binding and recognition,[3] chemical sensing,[4] light-emitting,[5] supramolecular catalysis,[6] synthetic ion channels,[7] molecular recognition and separation,[8] etc. Compared with other molecules or materials, the advantage of discrete SCCs such as coordination cages is their ability to form host−guest complexes through their finely tunable hollow cavities,[9] and they can be potentially used as nanocarriers for biological applications. However, there remain critical gaps in applying SCCs in real biological applications such as live-cell imaging, which is significant for the efficient and early diagnosis of cancer.[10] Basically, to our knowledge, there are still several issues to be overcome: (1) The limited structural stability of SCCs in harsh cellular environment. For example, most of the coordination cages are constructed by metal–ligand bonds (N→metal or O→metal). As a result, these cages have poor water stability, making them difficult to survive in living cellular environment.[11] (2) The weak fluorescence emission of SCCs in cellular environment. There are three possible reasons: (i) The aggregation caused quenching (ACQ) phenomenon[12] of SCCs strongly hampers the fluorescence when those SCCs aggregate together in the cellular environment. (ii) Some metal ions such as Fe (II), Cu (II), Co (II), and Ni (II) in the SCCs can easily self-quench the fluorescence due to their exceptionally short (sub-picosecond) ligand-to-metal charge transfer (LMCT) excited-state lifetimes.[13] (iii) Their fluorescence may be easily quenched by various biomolecules and components, such as amino acids, peptides, proteins, and serums in the complicated cellular environment. (3) The cell viability of SCCs is also a crucial problem for in-vitro biological applications.[14] Therefore, self-assembly of highly stable and strong emissive SCCs with low cytotoxic is still a synthetic challenge that, if overcome, could significantly expand the utility of SCCs in many biological applications.

We have shown previously that coordination cages built by trinuclear zirconium clusters are highly stable due to the high Zr-O bond energy (776 kJ mol^{-1}), showing excellent stability in aqueous solutions with acidic, neutral, and weak basic conditions.[15] We believe that this building unit can solve the stability problem of coordination cages in the cellular environment. For the second issue, Tang and co-workers have developed species that exhibit the opposite phenomenon called aggregation-induced emission (AIE),[16] which could offer strong fluorescence

[a] Dr. J. Dong,[+] Y. Pan,[+] Dr. K. Yang, Y. D. Yuan, S. B. Peh, Dr. J. Zhang, Dr. L. Shi, Prof. J. Jiang, Prof. B. Liu, Prof. D. Zhao
Department of Chemical and Biomolecular Engineering, National University of Singapore, 4 Engineering Drive 4, Singapore 117585
E-mail: chezhao@nus.edu.sg (D.Z.); cheliub@nus.edu.sg (B.L.)
[b] Dr. H. Wang, Prof. X. Li
Department of Chemistry, University of South Florida, Tampa, USA 33620
[c] Dr. L. Liu, Prof. Y. Han
King Abdullah University of Science and Technology (KAUST), Advanced Membranes and Porous Materials Center, Physical Sciences and Engineering Division, Thuwal, Saudi Arabia 23955-6900
[d] Prof. Z. Qiao, Prof. H. Liang
Guangzhou Key Laboratory for New Energy and Green Catalysis, School of Chemistry and Chemical Engineering, Guangzhou University, Guangzhou, P. R. China 510006
[+] These authors contributed equally to this work.

Supporting information for this article is given via a link at the end of the document.

10.1002/anie.201915199
WILEY-VCH

RESEARCH ARTICLE

upon molecular aggregation. Based on the AIE mechanism, we recently found that the dynamic phenyl rings of TPE core can work as AIE molecular rotors in porous materials,[17] which could be a good strategy to overcome the ACQ behavior in the cellular environment. Compared to our previous studies in which the AIE molecular rotors are anchored inside the cavities of porous organic frameworks (POFs),[17b-d] such molecular rotors exposed on the external surface of coordination cages would further manifest the expected AIE effect. Additionally, the TEP molecules contain four hydrophobic phenyl rings have limited interactions with biomolecules, leading to inhibition of quenching in the complicated cellular environment. For the third issue, we try to avoid toxic and self-quenching metal ions for the self-assembly of targeted coordination cages. With these design targets in mind, we envision that trinuclear zirconium (IV) cluster-based supramolecular coordination cages containing free rotary AIE molecular rotors would fulfill the above-mentioned requirements for biological applications.

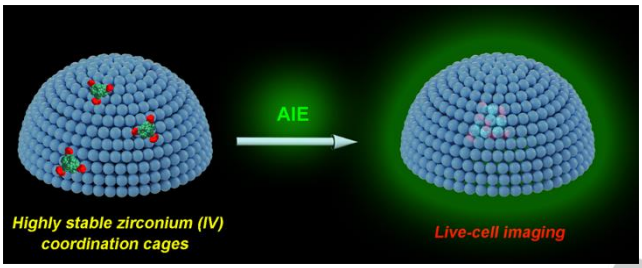

Scheme 1. Self-assembly of highly stable zirconium (IV) coordination cages containing AIE molecular rotors for live-cell imaging (red colour groups represent the AIE molecular rotors in the coordination cages).

In an effort to prove the above hypotheses, we herein demonstrate the first zirconium (IV) coordination cages with AIE molecular rotors that break the above limitations and yield novel biological probes for live-cell imaging (Scheme 1). Our strategy leverages the well-established TPE ligands with free phenyl rings as molecular rotors and carboxyl-decorated phenyl rings as stators to self-assemble highly stable Zr_6L_3 coordination cages. Our investigations show that the phenyl rings on the external surface of the coordination cages can function as AIE molecular rotors, leading to impressive AIE characteristics as proved by theoretical calculations and extensive experimental studies including temperature-responsive, viscosity-responsive, and guest size-responsive effects, as well as control experiments. Eventually, in-vitro cell culture assays suggest that these AIE molecular rotor-containing coordination cages are promising materials for live-cell imaging.

Results and Discussion

We began our studies with the design and synthesis of TPE ligands. As shown in Figure 1, the ligand H_2L_0 was synthesized according to the reported procedures (Figure S1 and S3a),[17a] and the longer ligand H_2L_1 was synthesized by the Suzuki-Miyaura couplings of 4,4'-(2,2-diphenylethene-1,1-diyl)bis(bromobenzene) and 4-(methoxycarbonyl)phenylboronic acid, followed by hydrolysis reaction (see SI for synthetic details,

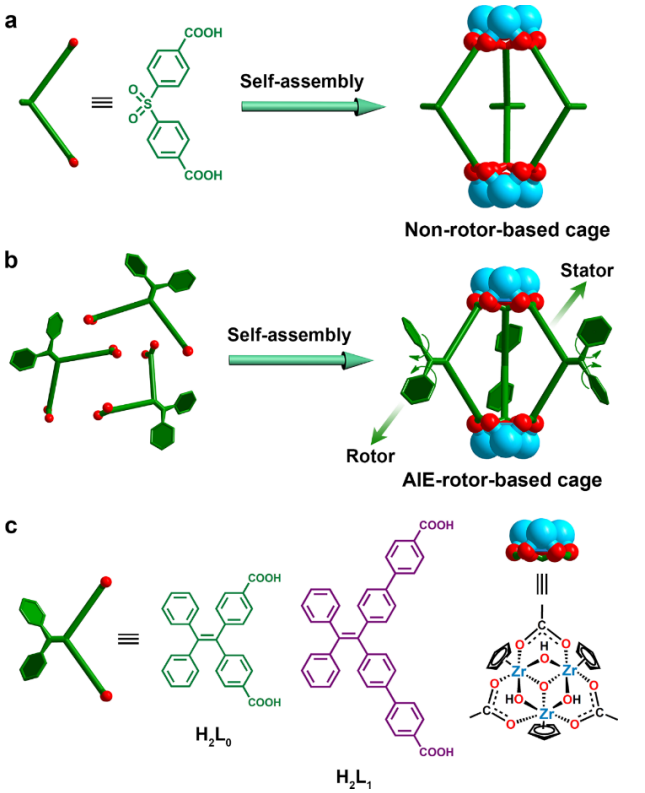

Figure 1. (a) Self-assembly of Zr_6L_3 coordination cage without AIE molecular rotors using 4,4'-sulfonyldibenzoic acid ligands. (b) Self-assembly of Zr_6L_3 coordination cages with AIE molecular rotors using flexible carboxyl-decorated TPE ligands. (c) The chemical structures of TPE ligands and trinuclear zirconium clusters used in this study.

Figure S2 and S3b). The single crystals of self-assembled coordination cages named NUS-100 (H_2L_0 ligand) and NUS-101 (H_2L_1 ligand) were obtained by heating bis(cyclopentadienyl)zirconium dichloride ($ZrCp_2Cl_2$) and H_2L_0 or H_2L_1 in *N*,*N*-dimethylformamide (DMF) at 65 °C for 12 h (Figure 1b-c), with the yields of 76% for NUS-100 and 64% for NUS-101. High-resolution electrospray ionization time-of-flight mass spectrometry (ESI-TOF-MS) was used to ascertain the correct molecular geometry of the self-assembled coordination cages. As expected, highly pure Zr_6L_3 supramolecular structures were identified as the target assemblies with the measured molecular weights of 2326 Da [experimental data at 1164.04 Da for $(M + 2H)^{2+}$] and 2782 Da [experimental data at 1392.11 Da for $(M + 2H)^{2+}$] for NUS-100 (Figure 2a) and NUS-101 (Figure 2b), respectively. In addition, the experimental isotopic patterns of two charge state of NUS-100 and NUS-101 are in good agreement with the simulated isotopic distributions (Inset of Figure 2a-b). Furthermore, the results of traveling wave ion mobility-mass spectrometry (TWIM-MS) show only one narrowly distributed signal band assigned to the $[M + 2H]^{2+}$ species of NUS 100-101, indicating the high purity of the two cages with no existence of other isomers or conformers. Moreover, we can observe that the drift time of NUS-101 (8.49 ms) is slightly longer than that of NUS-100 (6.28 ms) (Table S1), suggesting that the molecular size and

10.1002/anie.201915199

mass of NUS-101 is larger than that of NUS-100 (Figure S4). The cage for control experiments was self-assembled by 4,4'-sulfonyldibenzoic acid (H_2SDB) and $ZrCp_2Cl_2$ in DMF/H_2O at 65 °C (Figure 1a and Figure S5), which was previously reported as UCM-1.[18] In this study, we denoted it as non-rotor-based coordination cage (NR-cage), which has the same molecular geometry (Zr_6L_3) as that of NUS 100-101 (Figure S6-S7), with the difference that the six phenyl rings in NUS-100 or NUS-101 are replaced by six S=O groups in NR-cage. Such an isostructural Zr_6L_3 cage is beneficial to understanding the function of AIE molecular rotors in the coordination cages.

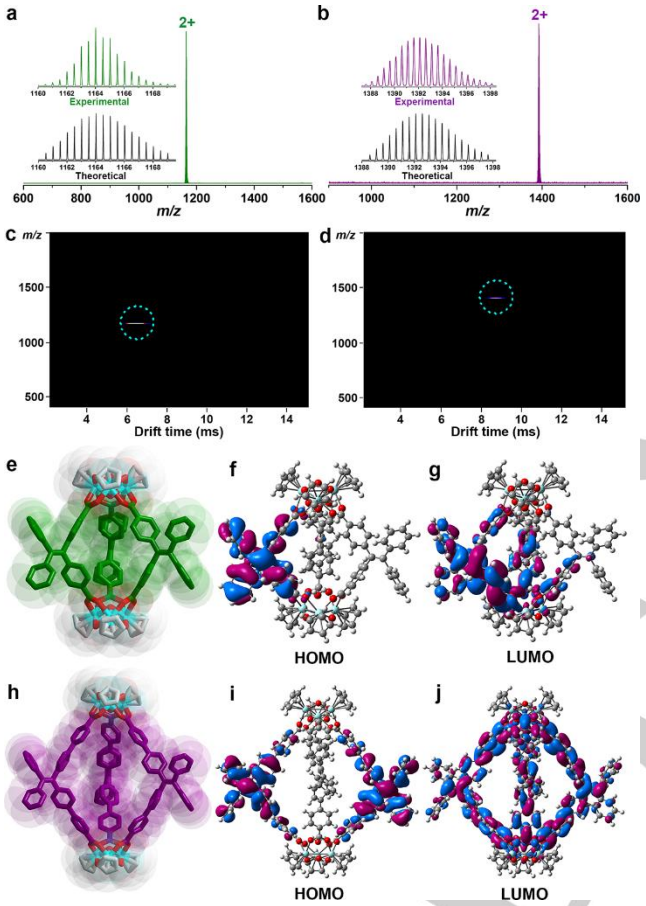

Figure 2. ESI-TOF-MS peaks of discrete NUS-100 (a) and NUS-101 (b). Inset: experimental and calculated isotope ESI-TOF-MS peaks. TWIM-MS plots of discrete NUS-100 (c) and NUS-101 (d). Minimum energy structures of NUS-100 (e) and NUS-101 (h) based on molecular dynamics simulations. Isodensity plots of the LUMO and HOMO of NUS-100 (f-g) and NUS-101 (i-j) based on TD-DFT calculations.

The formation of NUS 100-101 was confirmed by ^{1}H nuclear magnetic resonance (NMR) spectroscopy. Compared with the sharp ^{1}H-NMR signals of the TPE ligands (Figure 3a and 3c), the ^{1}H-NMR spectra of NUS 100-101 display slightly broadened peaks of all protons, due to their much slower tumbling motion on the NMR time scale. In addition, each cage displays only one set of NMR resonances in solution, suggesting the formation of discrete and highly symmetric assemblies (Figure 3b and 3d). However, most of these signals have slight upfield shifts with respect to the free ligands. For example, the proton resonance signals of phenyl rings at coordination part (H_a) of NUS-100 undergo a remarkable upfield shift (from 7.71 to 7.48 ppm, ΔH_a = – 0.23 ppm) with respect to H_2L_0. Such an upfield shift suggests that the free ligands are confined within the interlinked cage structure and thus experience a shielded magnetic environment.[5a] A similar upfield shift was observed in NUS-101. The quantitative formation of the two coordination cages was further confirmed via two-dimensional (2D) ^{1}H–^{1}H correlation spectroscopy (COSY) (Figure 3e-f) and ^{1}H–^{1}H nuclear Overhauser effect spectroscopy (NOESY) experiments (Figure S8), which show a single vertical trace in all cases. 2D diffusion-ordered spectroscopy (DOSY) experiments also confirm the formation of a single species with diffusion coefficients of 8.09 × 10^{-11} m^2 s^{-1} for NUS-100 (Figure 3g and Figure S9a) and 8.76 × 10^{-11} m^2 s^{-1} for NUS-101 (Figure 3h and Figure S9b), further suggesting that the Stokes−Einstein hydrodynamic radius of NUS-101 is larger than that of NUS-100, which is consistent with their geometry. Taken together, all the above NMR data indicate that the C_2-symmetry of TPE ligands are preserved in the Zr_6L_3 coordination cages.

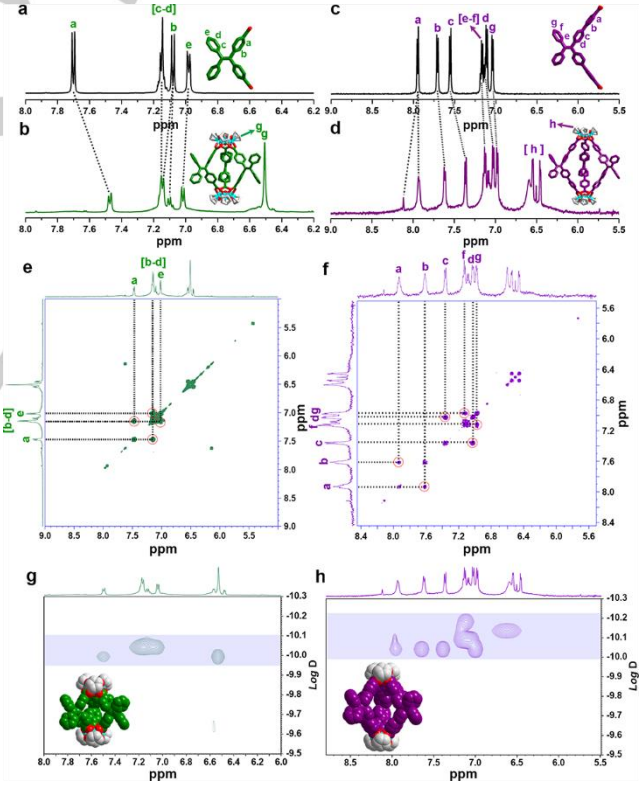

Figure 3. Partial ^{1}H NMR spectra of H_2L_0 (a), NUS-100 (b), H_2L_1 (c), and NUS-101 (d). 2D COSY spectra of NUS-100 (e) and NUS-101 (f). 2D DOSY spectra of NUS-100 (g) and NUS-101 (h).

Unfortunately, the weak X-ray diffraction limited the crystal structure determination in both cases. In this study, a low-dose (ca. 5 e-/Å^2) high-resolution transmission electron microscope (HR-TEM) technique[19] was employed to characterize the two coordination cages for avoiding electron beam-induced structural

10.1002/anie.201915199

damage (Figure 4c and 4f). Impressively, selected area electron diffraction (SAED) patterns show the rectangular patterns with strong diffraction in NUS-100 (Figure S10b), further confirming the high crystallinity of the cage. Moreover, the lattice fringes can be clearly observed from the obtained HR-TEM images in both cages, and the *d*-spacing values of around 1.47 nm for NUS-100 (Figure 4d) and 1.09 nm for NUS-101 (Figure 4g) match well with the XRD data (Figure S11). In addition, field-emission scanning electron microscopy (FE-SEM) show that the bulk crystals of these cages exhibit sheet-like morphology (Figure S12), and can be easily exfoliated into thin nanosheets in *n*-hexane (Figure S13). Quantitative measurements of their thickness were performed using atomic force microscopy (AFM), with the thicknesses of around 20 nm for NUS-100 (Figure 4e) and 15 nm for NUS-101 (Figure 4h).

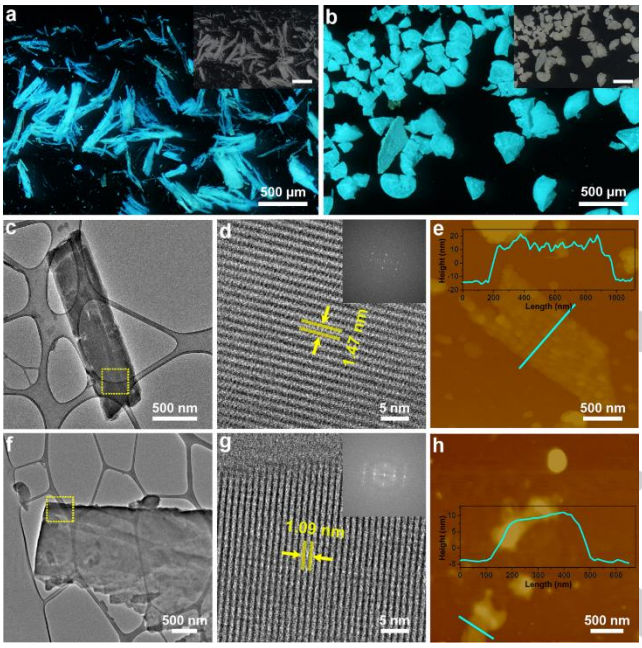

Figure 4. Fluorescence images of NUS-100 crystals (a) and NUS-101 crystals (b). Inset: optical images of NUS-100 and NUS-101 crystals, both scale bars are 500 μm. HR-TEM images of NUS-100 crystals (c) and NUS-101 crystals (f). HR-TEM images of NUS-100 crystals (d) and NUS-101 crystals (g) featuring the planar lattice structure. Inset: the fast Fourier transformation of Figure (d) and (g). AFM images of as-exfoliated nanosheets of NUS-100 (e) and NUS-101 (h).

NUS 100-101 were further characterized by various spectroscopic methods. X-ray photoelectron spectroscopy (XPS) spectra show the presence of Zr (Zr 3d: 182 eV) and O (O 1s: 532 eV) elements in both cages (Figure S14). In addition, the corresponding energy-dispersive X-ray (EDX) spectroscopy mapping indicates that there are homogeneous distributions of Zr and O elements in the crystals (Figure S15-S16), which is consistent with XPS data. Fluorescence images show that the two cage crystals exhibit cyan emission (Figure 4a-b). Furthermore, we performed 3D confocal laser scanning microscopy (CLSM) to observe the anisotropic behavior of the fluorescence of the two cage crystals, unveiling the homogeneous strong emissions in the whole crystals (Figure S17-S18). Fluorescence emission spectra show that NUS-100 and NUS-101 have blue-shifts of around 25 and 22 nm compared to H_2L_0 and H_2L_1 in the solid-state (Figure S19-S20), respectively. UV-Vis spectra show that NUS-100 and NUS-101 have 31 and 3 nm blue-shifts than H_2L_0 (λ_{max} = 309 nm) and H_2L_1 (λ_{max} = 319 nm) (Figure S21-S22), respectively. To gain insight into the electronic property of the two cages, time dependent density functional theory (TD-DFT) calculations were performed to understand their transition from the highest energy occupied molecular orbital (HOMO) to the lowest unoccupied molecular orbital (LUMO) (Figure 2f-g, Figure 2i-j, and Figure S23-S25). TD-DFT results indicate that when the ligand coordinates with metal to form cage complexes, the interplay becomes complicated. The transition of HOMO→LUMO only contributes about 20% and 10% to the absorption peak of NUS-100 (λ_{max} = 301 nm) and NUS-101 (λ_{max} = 332 nm), respectively, which are much smaller than their ligands (see more details and explanations in Table S2-S5). Other information such as Fourier transform infrared spectra (FT-IR), thermogravimetric analyses (TGA), and corresponding optical band gaps (E_g) are shown in the supporting information (Figure S26-S28).

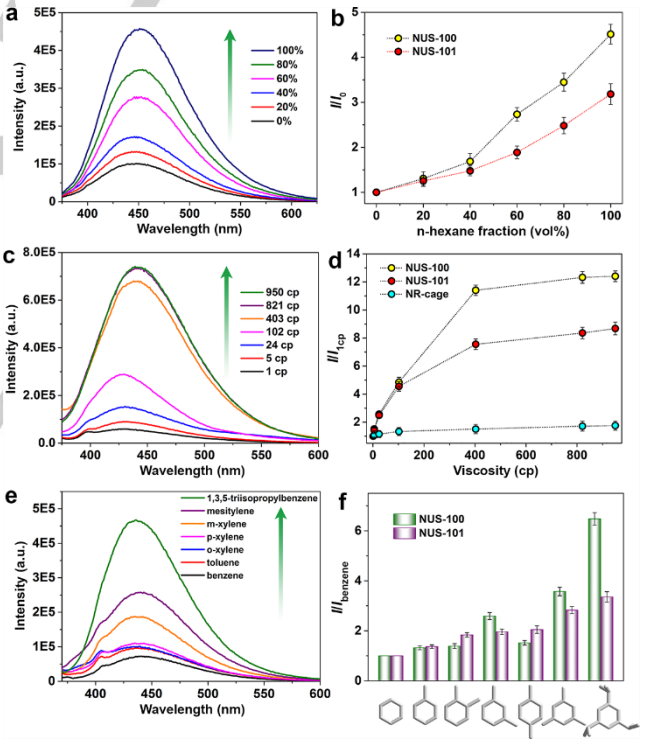

Figure 5. (a) Fluorescence emission spectra of NUS-100 versus *n*-hexane fraction in CH_2Cl_2/*n*-hexane mixtures. (b) Plot of relative emission intensity (I/I_0) of NUS 100-101 in CH_2Cl_2/*n*-hexane mixtures. (c) Fluorescence emission spectra of NUS-100 in solutions of various viscosities. (d) Plot of relative emission intensity (I/I_{1cp}) of NUS 100-101 with various viscosities. (e) Fluorescence emission spectra of NUS-100 in various VOC solutions with different molecular sizes. (f) Relative fluorescence intensity ($I/I_{benzene}$) of NUS 100-101 in various VOC solutions. The concentrations of NUS 100-101 are 1.0 × 10^{-5} M, and the excitation wavelength is 360 nm in the experiments.

10.1002/anie.201915199

To have a better understanding on the dynamic behavior of the phenyl ring rotors located on the external surface of the two coordination cages, the AIE characteristics of NUS 100-101 were studied in mixtures of dichloromethane (CH_2Cl_2) and *n*-hexane.[5a] As expected, both cages exhibit typical AIE characteristics. As shown in Figure 5a, the fluorescence intensity of NUS-100 is substantially enhanced with increasing *n*-hexane fraction (f_h). The highest fluorescence intensities were obtained at f_h of 100% for NUS-100 and NUS-101, and are 4.51- and 3.18-fold higher than that in CH_2Cl_2 solutions (Figure S29a and Figure 5b), respectively. However, the NR-cage exhibits a slightly reduced fluorescence intensity at f_h of 100%, with is only 0.90-fold of that in CH_2Cl_2 solution (Figure S30a). Such a typical AIE phenomenon of NUS 100-101 can be attributed to the restriction of phenyl ring rotors of the cages in their aggregated state. Next, various stimuli were applied to evaluate the sensitivity of AIE molecular rotors of the two cages. First of all, it is known that fluorescent molecular rotors with the nonradiative decay of their excited state is influenced by the viscosity of the medium.[20] Therefore, fluorescence measurements of the two cages were made in DMF/glycerol mixtures with different viscosities. As expected, when the viscosity is increased to 950 cp (99% glycerol solution), the emission intensity of NUS-100 greatly enhances by 12.40-fold ($I_E = I_{950cp}/I_{1cp}$) compared to that in DMF solution (1 cp) (Figure 5c-d). A similar trend of I_E was found in NUS-101 with a value of 8.68-fold (Figure S29b and Figure 5d). The control experiments show that the I_E value (1.76) of NR-cage is much lower from DMF to glycerol solution (Figure S31 and Figure 5d). These results unambiguously indicate that such highly-stable coordination cages equipped with AIE molecular rotors are highly sensitive to environmental viscosity, which can be contributed to the restricted rotation of the AIE molecular rotors preventing relaxation via populating of the dark excited state.

Second, the two cages exhibit different fluorescence emissions after soaking in various volatile organic compounds (VOCs) with size-dependent effect. Using the emission intensity of cages being soaked in benzene ($I_{benzene}$, 4.3 × 5.0 Å) as the reference, we evaluated the relative intensity ($I_R = I/I_{benzene}$) of the cages in different analytes, such as toluene (4.3 × 5.9 Å), *o*-xylene (5.5 × 5.9 Å), *m*-xylene (5.0 × 6.7 Å), *p*-xylene (4.3 × 6.8 Å), mesitylene (5.8 × 6.7 Å), and 1,3,5-triisopropylbenzene (8.4 × 9.0 Å).[17c] A clear positive correlation between I_R values versus molecular size of the analytes can be found (Figure 5e and Figure S29c). Taking NUS-100 as an example, the I_R values of NUS-100⊃benzene, NUS-100⊃toluene, NUS-100⊃*p*-xylene, and NUS-100⊃mesitylene are 1.00, 1.32, 1.52, and 3.57 (Figure 5f), respectively. A similar trend was also observed in NUS-101 (1.00, 1.37, 2.05, and 2.83, respectively). We speculated that the size-dependent turn-on fluorescence of the two cages is due to the different restriction degrees of the phenyl ring rotors. To prove this point, we used 1,3,5-triisopropylbenzene as a large analyte to see if the phenyl ring rotors of the cages can be further restricted for higher fluorescence emission. As shown in Figure 5f, the I_R values of NUS-100⊃1,3,5-triisopropylbenzene (I_R = 6.48) and NUS-101⊃1,3,5-triisopropylbenzene (I_R = 3.36) are much higher than that in other VOC solutions, suggesting the size-dependent restricted effect for the molecular rotors. Our previous study indicates that the emission intensities of POFs NUS 20-23 in 1,3,5-triisopropylbenzene are much lower than that in mesitylene because the pore sizes of these POFs are too small for the incorporation and interaction of 1,3,5-triisopropylbenzene.[17b] Surprisingly, we observed the sustained increase of emission intensity in 1,3,5-triisopropylbenzene solution in this study (Figure 5f). This is because the molecular rotors located at the external surface of the cages have free access to analytes, which is different from the confined molecular rotors located inside the pores of those POFs. In addition, the I_R value of NR-cage⊃1,3,5-triisopropylbenzene is only 1.28 (Figure S30b), which is much smaller than that of the two cages. Our findings unambiguously indicate that the dynamic molecular rotors of the cages can be restricted by guest molecules with size-dependent effect.

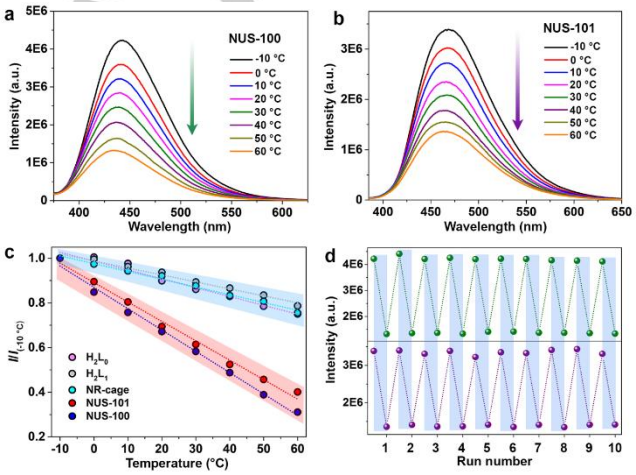

Figure 6. Temperature-responsive emissions of NUS-100 (a) and NUS-101 (b) in THF solutions recorded between −10 and 60 °C. (c) Relative fluorescence intensity ($I/I_{-10\ °C}$) of NUS 100-101, TPE ligands, and NR-cage under various temperatures. (d) Cyclic switching (10 times) of fluorescence intensity upon heating and cooling for NUS-100 (top) and NUS-101 (bottom) in THF solutions. The concentrations of NUS 100-101 are 5.0 × 10^{-5} M, and the excitation wavelength is 360 nm in the experiments.

Third, temperature-responsive fluorescence is also a typical characteristic of molecular rotors.[21] In order to prove this, we tested the temperature-responsive fluorescence of the two cages. As shown in Figure 6a-b, upon increasing temperature from -10 to 60 °C, the emission intensities of NUS 100-101 significantly decrease. This is because rotations of the phenyl ring rotors are expected to speed up upon increasing temperature, which can lead to the disruption of charge-transfer and consumption of energy with reduced fluorescence emissions.[21b] In particular, the emission intensities of NUS 100-101 drop by 68.9% and 59.9%, respectively, over this temperature range. Furthermore, the temperature-dependent emission responses of NUS 100-101 can be fitted with linear functions, with average slopes of -0.96% and -0.87% per °C, respectively. Moreover, the control experiment shows that the decrease in emission intensity of NR-cage is only

10.1002/anie.201915199

24.5% with an average slope of -0.35% per °C over this temperature range (Figure S32 and Figure 6c), which is also much smaller than that of NUS 100-101, highlighting the sensitivity of phenyl ring rotors toward temperature. In addition, although we observed the same trend in the ligands upon increasing temperature, the drop degrees of H_2L_0 and H_2L_1 are 25.0% and 21.3%, respectively, Similarly, the average slopes of the linear functions of the two ligands are also much smaller (-0.40% and -0.31% per °C for H_2L_0 and H_2L_1, respectively) than that of the cages (Figure S33 and Figure 6c). These results reveal that the dynamic molecular rotors in the cages are more sensitive than in the free ligands. Impressively, the temperature cycling experiments indicate highly reversible rotation of phenyl ring rotors under temperature control over ten runs attempted (Figure 6d and Figure S34-S35), highlighting that the dynamic AIE molecular rotors can operate effectively in the highly stable coordination cages.

To further understand the temperature response of AIE molecular rotors in the two cages, we performed the variable-temperature ^{1}H-NMR experiments to test any possible proton signal change for the phenyl ring rotors of NUS 100-101. As expected, we can clearly observe that the proton signals of the phenyl ring rotors (H_e in NUS-100 and H_g in NUS-101) exhibit downfield shifts from 25 to 65 °C, with ΔH_e of 0.04 ppm in NUS-100 and ΔH_g of 0.02 ppm in NUS-101 (Figure 7a-b), confirming the faster rotary speed of the phenyl ring rotors under higher temperatures.[21b] Combined with viscosity-responsive, guest size-dependent-responsive, and temperature-responsive fluorescence change behaviors, the above results strongly confirm the existence of dynamic molecular rotors in the coordination cages.

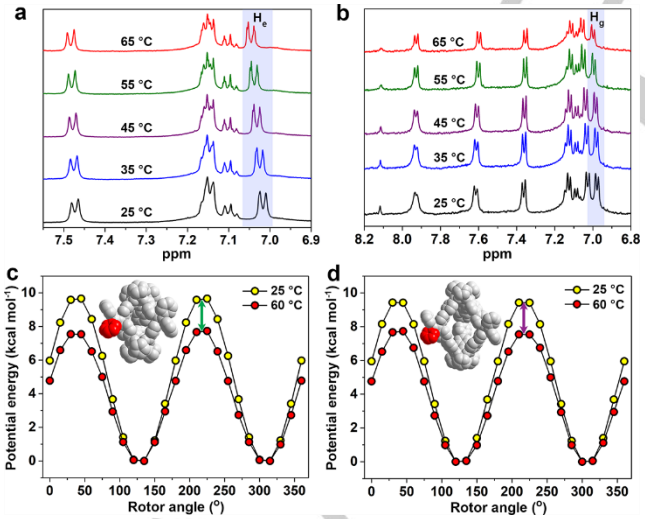

Figure 7. Partial ^{1}H NMR spectra of NUS-100 (a) and NUS-101 (b) at different temperatures. The theoretical calculations of energy barriers of phenyl ring rotors (red color in molecular models) in NUS-100 (c) and NUS-101 (d) at 25 or 60 °C.

Given the significance of the above findings, it is essential to elucidate why the phenyl ring rotors have such a dynamic behavior. Accordingly, we performed molecular dynamics (MD) simulations to estimate the rotational energy barriers of phenyl ring rotors of NUS 100-101. Figure 7c-d show the potential energy of one phenyl ring rotor of each cage as a function of rotor angle varying from 0 to 360° with an interval of 15°, in which two stable conformations were observed at around 135 and 315°. On the contrary, less favorable conformations could be observed at around 45 and 225° with relative higher energy barriers. The rotation energy barriers were calculated to be 9.66 kcal mol^{-1} in NUS-100 and 9.42 kcal mol^{-1} in NUS-101 at 25 °C, which are lower than that of the confined molecular rotors in our previous POFs NUS-24 (14.0 kcal mol^{-1})[17c] and NUS-25 (12.1 kcal mol^{-1}).[17d] Moreover, we performed the potential energy calculations for one phenyl ring rotor under 60 °C, and obtained the similar trend of the potential energy with 25 °C. However, the rotation energy barriers decrease to 7.54 kcal mol^{-1} in NUS-100 and 7.73 kcal mol^{-1} in NUS-101 (Figure 7c-d), indicating that the phenyl ring rotors are sensitive to temperature. Therefore, the computational and experimental results are consistent and reasonable to interpret the nonradiative energy release pathways of the cages via multiple external stimuli-responsive environments.

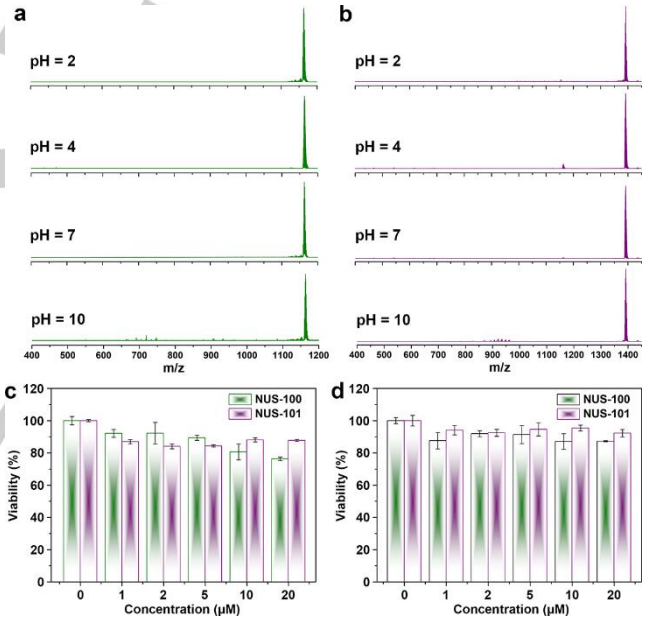

Figure 8. ESI-TOF-MS spectra of NUS-100 (a) and NUS-101 (b) in methanol/water solutions with different pH values. The cytotoxicity assay results of NUS-100 and NUS-101 in NIH-3T3 cells (c) and HeLa cells (d).

The suitable molecular size and AIE fluorescence behavior of NUS 100-101 prompt us to evaluate their feasibility as molecular fluorescent probes in live-cell imaging. We initially studied their structural stability, fluorescence emission, and cytotoxicity in aqueous solutions, which are the prerequisites for in-vitro bio-imaging. Impressively, NUS 100-101 are highly stable in aqueous solutions with acidic, neutral, and weak basic conditions, confirmed by the ESI-TOF-MS data of their aqueous solutions with pH values from 2 to 10 (Figure 8a-b). Furthermore, fluorescence emission spectra of the two cages keep unchanged under similar conditions (Figure S36-S37). In addition, time-

10.1002/anie.201915199

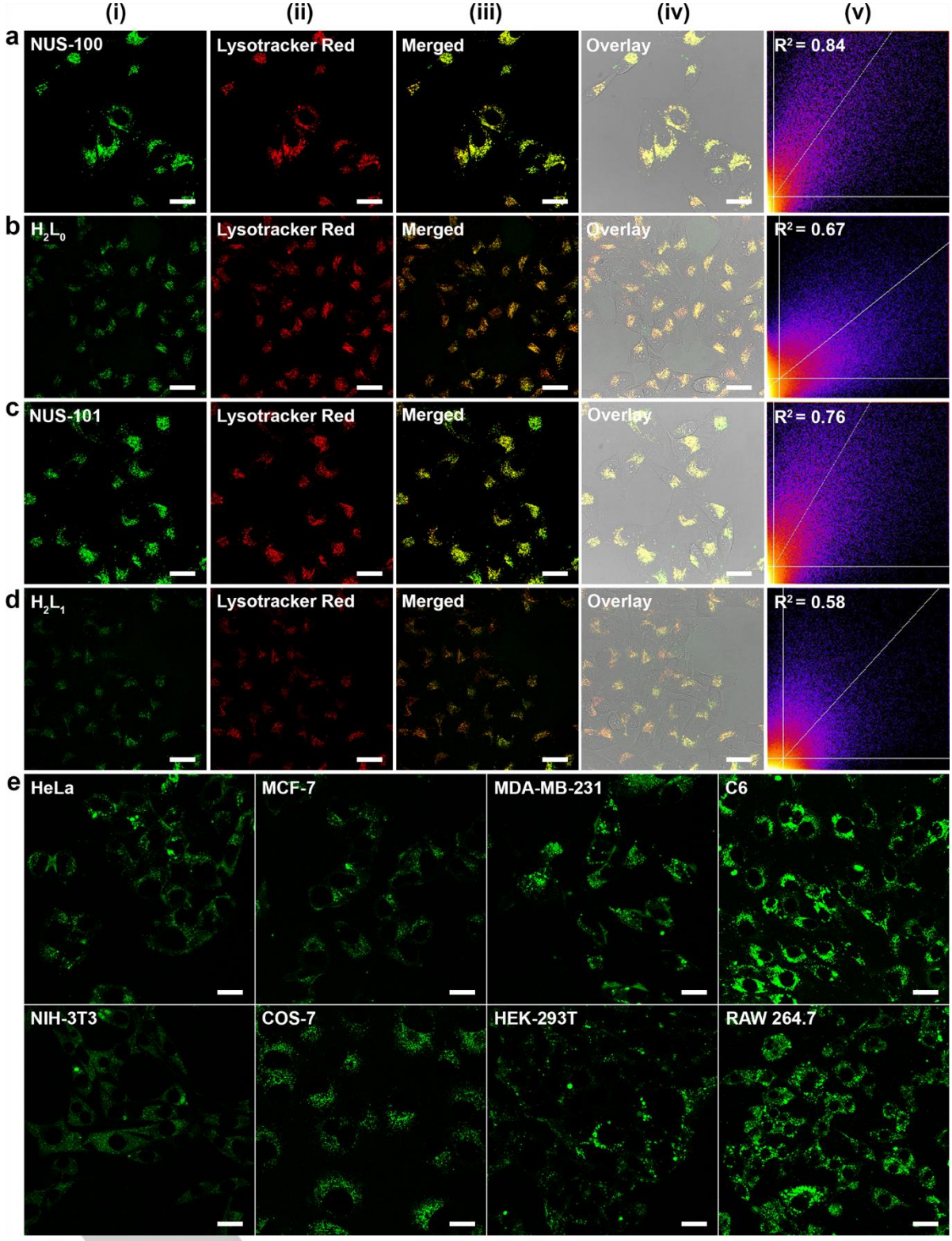

Figure 9. The CLSM imaging in HeLa cells using NUS-100 (a), H_2L_0 (b), NUS-101 (c), and H_2L_1 (d) compared with Lysotracker Red after 24 h incubation. (i) HeLa cells CLSM images. (ii) Lysotracker Red images. (iii) Colocalized images. (iv) Overlay images with bright field. (v) Scatter plots and Pearson's R values. (e) The CLSM imaging in four cancerous cells and four non-cancerous cells using NUS-100 under the same conditions. All scale bars are 20 μm.

resolved photoluminescence measurement (TRPL) results show that the lifetimes of NUS-100 and NUS-101 are 0.97 and 1.03 ns at neutral aqueous solutions (Figure S38), respectively, and the quantum yields (QY) of NUS-100 and NUS-101 under neutral

aqueous solutions were determined to be 19.0 ± 1% and 28.8 ± 1%, respectively. Importantly, cell viability assay of NUS 100-101 was conducted in NIH-3T3 and HeLa cell lines by incubating for 24 h at concentrations ranging from 1 μM to 20 mM by methylthiazolyldiphenyltetrazolium bromide (MTT) method.[14] As shown in Figure 8c-d, no significant toxicity was noted in both two cell lines with viabilities higher than 80% under all conditions. All these data indicate that the two coordination cages have high stability, strong fluorescence, and low cytotoxicity, making them suitable candidates for in-vitro bio-imaging applications.

Inspired by the above results, NUS 100-101 were further applied into HeLa cell line to evaluate their imaging capabilities. After incubating for 24 h at 10 μM, strong signals from inside cytoplasm region were observed in CLSM images (Figure 9a and 9c, Figure S39). Notably, non-specific targeting nanomaterials tend to be internalized through endocytosis, and lysosomes are the last compartment of the endocytic pathway, leading to distribution of nanomaterials in lysosomes. The location of signal was further studied by colocalization analysis with Lysotracker™ Red DND-99. The Pearson's R values for NUS-100 and NUS-101 are 0.84 and 0.76, respectively, indicating the major distribution in lysosomes. The internalization process was captured by time lapse imaging using live-imaging chamber. Signal intensity gradually increased from 6 to 24 h with very few aggregates outside cells, showing excellent imaging ability (Figure S40-S41). Additionally, H_2L_0 and H_2L_1 were also incubated with HeLa cells for 24 h to compare the imaging capability between ligands and cages (Figure 9b and 9d). CLSM images were taken under the same conditions followed by colocalization analysis, showing much weaker fluorescence and lower Pearson's R values for H_2L_0 (Figure 9b) and H_2L_1 (Figure 9d). Moreover, NUS-100 and NUS-101 can also be applied into imaging of MCF-7 and MDA-MB-231 cancerous cells, as well as NIH-3T3 normal cells (Figure S42-S43). In order to illustrate the universal live-cell imaging ability of the cages, we took NUS-100 as an example and investigated a broader live-cell imaging screening for four cancerous cells including HeLa, MCF-7, MDA-MB-231 and C6, and four non-cancerous cells such as COS-7, NIH-3T3, HEK-293T and one macrophage cells RAW 264.7 under the same conditions (Figure S44). As shown in Figure 9e, CLSM images showed that both cancerous cells and non-cancerous cells are bright, indicating that the AIE-active cages are potential fluorescent probes to universally label a wide range of cell lines. However, due to the difference in endocytosis abilities and the different intracellular environment (i.e., different viscosity), the fluorescence intensity varies in different cell lines. Furthermore, we also performed the control experiment of HeLa cells imaging using NR-cage, which exhibited much weaker imaging than that of NUS 100-101 (Figure S45-S46), further highlighting that the AIE molecular rotors in NUS 100-101 are beneficial for live-cell imaging. Our findings have successfully demonstrated the universal live-cell imaging using highly stable and fluorescent zirconium (IV) coordination cages with AIE molecular rotors, paving the way for the biological applications of these coordination cages.

Conclusion

In summary, we have designed and synthesized highly stable zirconium (IV)-based coordination cages containing AIE molecular rotors for live-cell imaging. The phenyl ring rotors located on the external surface of the coordination cages can be effectively restricted by various stimuli, including temperature, viscosity, and guests with various molecular sizes, leading to strong AIE characteristics. Such highly stable and fluorescent supramolecular coordination cages show the following advantages over other supramolecular coordination assemblies in biological applications: (1) high stability in cellular environment, (2) bright fluorescence based on the impressive AIE characteristics, and (3) low cytotoxicity suitable for biological applications. As a proof-of-concept study, we have successfully applied the two cages for universal live-cell imaging. We envision that such zirconium (IV)-based fluorescent coordination cages have potential applications in various biological applications including diagnosis of living cancer cells, drug delivery, and photodynamic therapy.

Experimental Section

Experimental details on the synthesis and characterization of H_2L_0, H_2L_1, and NUS 100-101, AIE experiments, temperature-response, viscosity-response, and size-effect of guest molecules, in-vitro cancer cell imaging, MD simulations and TD-DFT calculations are provided in the Supplementary Information.

Acknowledgements

This work was supported by the National Research Foundation Singapore (NRF2018-NRF-ANR007 POCEMON), the Ministry of Education - Singapore (MOE AcRF Tier 1 R-279-000-540-114, R-279-000-482-133, Tier 2 MOE2018-T2-2-148), the Agency for Science, Technology and Research (IRG A1783c0015, IAF-PP A1789a0024), National Natural Science Foundation of China (No. 21676094 and 21576058), Fundamental Research Funds for the Central Universities (2017MS083), and the technical support from National Supercomputer Center in Guangzhou (Tianhe-2).

Keywords: self-assembly • coordination cage • aggregation induced emission • molecular rotor • live-cell imaging

[1] a) T. R. Cook, Y.-R. Zheng, P. J. Stang, *Chem. Rev.* **2013**, *113*, 734-777. b) T. R. Cook, P. J. Stang, *Chem. Rev.* **2015**, *115*, 7001-7045. c) W. Wang, Y.-X. Wang, H.-B. Yang, *Chem. Soc. Rev.* **2016**, *45*, 2656-2693.

[2] a) L. Xu, Y.-X. Wang, L.-J. Chen, H.-B. Yang, *Chem. Soc. Rev.* **2015**, *44*, 2148-2167. b) K. L. Haas, K. J. Franz, *Chem. Rev.* **2009**, *109*, 4921-4960.

[3] a) D. Zhang, T. K. Ronson, J. Mosquera, A. Martinez, L. Guy, J. R. Nitschke, *J. Am. Chem. Soc.* **2017**, *139*, 6574-6577. b) A. B. Grommet, J. B. Hoffman, E. G. Percástegui, J. Mosquera, D. J. Howe, J. L. Bolliger, J. R. Nitschke, *J. Am. Chem. Soc.* **2018**, *140*, 14770-14776.

[4] a) M. Zhang, M. L. Saha, M. Wang, Z. Zhou, B. Song, C. Lu, X. Yan, X. Li, F. Huang, S. Yin, P. J. Stang, *J. Am. Chem. Soc.* **2017**, *139*, 5067-5074. b)

J. Dong, C. Tan, K. Zhang, Y. Liu, P. J. Low, J. Jiang, Y. Cui, *J. Am. Chem. Soc.* **2017**, *139*, 1554-1564. c) J. Dong, Y. Zhou, F. Zhang, Y. Cui, *Chem. - Eur. J.* **2014**, *20*, 6455-6461.

[5] a) X. Yan, T. R. Cook, P. Wang, F. Huang, P. J. Stang, *Nat. Chem.* **2015**, *7*, 342-348. b) X. Yan, M. Wang, T. R. Cook, M. Zhang, M. L. Saha, Z. Zhou, X. Li, F. Huang, P. J. Stang, *J. Am. Chem. Soc.* **2016**, *138*, 4580-4588.

[6] a) Y. Ueda, H. Ito, D. Fujita, M. Fujita, *J. Am. Chem. Soc.* **2017**, *139*, 6090-6093. b) H. Takezawa, T. Kanda, H. Nanjo, M. Fujita, *J. Am. Chem. Soc.* **2019**, *141*, 5112-5115. c) C. J. Brown, F. D. Toste, R. G. Bergman, K. N. Raymond, *Chem. Rev.* **2015**, *115*, 3012-3035. d) J. Jiao, C. Tan, Z. Li, Y. Liu, X. Han, Y. Cui, *J. Am. Chem. Soc.* **2018**, *140*, 2251-2259.

[7] a) N. Sakai, S. Matile, *Angew. Chem., Int. Ed.* **2008**, *47*, 9603-9607; *Angew. Chem.* **2008**, *120*, 9745-9749. b) M. Jung, H. Kim, K. Baek, K. Kim, *Angew. Chem. Int. Ed.* **2008**, *47*, 5755-5757; *Angew. Chem.* **2008**, *120*, 5839-5841.

[8] a) G. Li, W. Yu, Y. Cui, *J. Am. Chem. Soc.* **2008**, *130*, 4582-4583. b) K. Wu, K. Li, Y.-J. Hou, M. Pan, L.-Y. Zhang, L. Chen, C.-Y. Su, *Nat. Commun.* **2016**, *7*, 10487.

[9] a) P. Mal, B. Breiner, K. Rissanen, J. R. Nitschke, *Science* **2009**, *324*, 1697-1699. b) B. Chen, J. J. Holstein, S. Horiuchi, W. G. Hiller, G. H. Clever, *J. Am. Chem. Soc.* **2019**, *141*, 8907-8913. c) K. Yazaki, M. Akita, S. Prusty, D. K. Chand, T. Kikuchi, H. Sato, M. Yoshizawa, *Nat. Commun.* **2017**, *8*, 15914. d) X. Jing, C. He, Y. Yang, C. Duan, *J. Am. Chem. Soc.* **2015**, *137*, 3967-3974.

[10] G. Feng, B. Liu, *Acc. Chem. Res.* **2018**, *51*, 1404-1414.

[11] Y. Fang, X. Lian, Y. Huang, G. Fu, Z. Xiao, Q. Wang, B. Nan, J.-P. Pellois, H.-C. Zhou, *Small* **2018**, **14**, 1802709.

[12] R. Hu, N. L. C. Leung, B. Z. Tang, *Chem. Soc. Rev.* **2014**, *43*, 4494-4562.

[13] a) C. Creutz, M. Chou, T. L. Netzel, M. Okumura, N. Sutin, *J. Am. Chem. Soc.* **1980**, *102*, 1309-1319.

[14] J. Zhou, Y. Zhang, G. Yu, M. R. Crawley, C. R. P. Fulong, A. E. Friedman, S. Sengupta, J. Sun, Q. Li, F. Huang, T. R. Cook, *J. Am. Chem. Soc.* **2018**, *140*, 7730-7736.

[15] G. Liu, Y. Di Yuan, J. Wang, Y. Cheng, S. B. Peh, Y. Wang, Y. Qian, J. Dong, D. Yuan, D. Zhao, *J. Am. Chem. Soc.* **2018**, *140*, 6231-6234.

[16] a) J. Luo, Z. Xie, J. W. Y. Lam, L. Cheng, H. Chen, C. Qiu, H. S. Kwok, X. Zhan, Y. Liu, D. Zhu, B. Z. Tang, *Chem. Commun.* **2001**, 1740-1741. b) Y. Hong, J. W. Y. Lam, B. Z. Tang, *Chem. Soc. Rev.* **2011**, *40*, 5361-5388. c) J. Mei, N. L. C. Leung, R. T. K. Kwok, J. W. Y. Lam, B. Z. Tang, *Chem. Rev.* **2015**, *115*, 11718-11940.

[17] a) M. Zhang, G. Feng, Z. Song, Y.-P. Zhou, H.-Y. Chao, D. Yuan, T. T. Y. Tan, Z. Guo, Z. Hu, B. Z. Tang, B. Liu, D. Zhao, *J. Am. Chem. Soc.* **2014**, *136*, 7241-7244. b) J. Dong, A. K. Tummanapelli, X. Li, S. Ying, H. Hirao, D. Zhao, *Chem. Mater.* **2016**, *28*, 7889-7897. c) J. Dong, K. Zhang, X. Li, Y. Qian, H. Zhu, D. Yuan, Q.-H. Xu, J. Jiang, D. Zhao, *Nat. Commun.* **2017**, *8*, 1142. d) J. Dong, X. Li, K. Zhang, Y. Di Yuan, Y. Wang, L. Zhai, G. Liu, D. Yuan, J. Jiang, D. Zhao, *J. Am. Chem. Soc.* **2018**, *140*, 4035-4046.

[18] S. Lee, J. H. Lee, J. C. Kim, S. Lee, S. K. Kwak, W. Choe, *ACS Appl. Mater. Inter.* **2018**, *10*, 8685-8691.

[19] D. Zhang, Y. Zhu, L. Liu, X. Ying, C.-E. Hsiung, R. Sougrat, K. Li, Y. Han, *Science* **2018**, *359*, 675-679.

[20] a) M. K. Kuimova, G. Yahioglu, J. A. Levitt, K. Suhling, *J. Am. Chem. Soc.* **2008**, *130*, 6672-6673. b) L. Wang, Y. Xiao, W. Tian, L. Deng, *J. Am. Chem. Soc.* **2013**, *135*, 2903-2906.

[21] a) M. Jin, T. S. Chung, T. Seki, H. Ito, M. A. Garcia-Garibay, *J. Am. Chem. Soc.* **2017**, *139*, 18115-18121. b) J.-H. Tang, Y. Sun, Z.-L. Gong, Z.-Y. Li, Z. Zhou, H. Wang, X. Li, M. L. Saha, Y.-W. Zhong, P. J. Stang, *J. Am. Chem. Soc.* **2018**, *140*, 7723-7729.

10.1002/anie.201915199

WILEY-VCH

RESEARCH ARTICLE

We report the self-assembly of highly stable coordination cages from the trinuclear zirconium vertices and flexible carboxyl-decorated tetraphenylethylene (TPE) spacers. The two water-stable cages exhibit impressive aggregation induced emission (AIE) characteristics contributed by the molecular rotors, and can be employed as novel biological fluorescent probes for live-cell imaging.

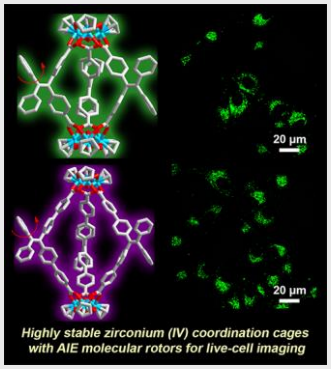

Dr. Jinqiao Dong, Yutong Pan, Dr. Heng Wang, Dr. Kuiwei Yang, Dr. Lingmei Liu, Prof. Zhiwei Qiao, Yi Di Yuan, Shing Bo Peh, Dr. Jian Zhang, Dr. Leilei Shi, Prof. Hong Liang, Prof. Yu Han, Prof. Xiaopeng Li, Prof. Jianwen Jiang, Prof. Bin Liu, and Prof. Dan Zhao**

Page No. – Page No.

Self-Assembly of Highly Stable Zirconium (IV) Coordination Cages with Aggregation Induced Emission (AIE) Molecular Rotors for Live-Cell Imaging